Ninth International Conference on Computational Fluid Dynamics (ICCFD9), Istanbul, Turkey, July 11-15, 2016

ICCFD9-xxxx

A Numerical Study of Circulation Control on a Flapless UAV

Huaixun Ren[1], Weimin Cai[2], Lihua Gao [1] & Yong Huang[1]

[1]Low Speed Aerodynamics Institute, China Aerodynamics Research and Development Center, Mianyang 622762, China

[2] Shenyang Aircraft Design & Research Institute, Shenyang 110035, China

Corresponding author: renhuaixun@163.com

Abstract: Reynolds-averaged Navier–Stokes (RANS) simulations of circulation control (CC) for provision of three-axis moments on a flapless unmanned aerial vehicle (UAV) are carried out using the finite volume method (FVM) for spatial discretisation. Validation was conducted against the experiment performed on NCCR 1510-7067N elliptical circulation control airfoil with SST turbulence model, which was shown to have considerably good capability of predicting the features of Coanda wall jet flows. Further, the effect of the location of jet unit on the moment characteristics of the vehicle is investigated. It can be revealed that blowing from upper and lower CC slots at the same spanwise position produce opposite, basically same offset values of pitching and rolling moments for the same set of values of parameters: momentum coefficient C_μ and total temperature in the plenum T_j. Independent rolling or pitching moment could be realized by blowing with a certain arrangement of the locations of CC slots at both sides of the wing, and the increments of pitching and rolling moments caused by blowing are mostly provided by the jet unit closest to the wing root. Moreover, yawing moment can also be generated by simultaneous blowing from upper and lower CC slots close to the wing tip, which induces the increase of local axial force.

Keywords: Circulation Control, flapless UAV, blowing, pitching and rolling moments.

1 Introduction

Coanda effect is about the fact that wall-bounded jet tends to remain attached to the curved surface. Circulation Control (CC), taking advantage of Coanda effect, can significantly increase the lift of airfoil, which has great potential in improving aircraft aerodynamic performance [1,2]. When circulation control is imposed, high pressure gas is injected along the direction tangential to wall at or nearby the trailing edge of airfoil, and this wall-bounded jet will drive the outflow to be attached to the airfoil surface due to Coanda effect. This attached flow produces very large circulation, and thus enhances the maximum lift of airfoil substantially [3]. Compared with traditional control surfaces, CC technology, which makes the mechanical structure used for maneuvering manipulating of aircraft simplified, has great advantages in lift enhancement, vibration noise suppression, etc.

In recent years, CC has been widely studied and applied in the field of aviation. Powered lift, under-the-wing blowing or upper-surface blowing to raise the maximum lift coefficient, increases the energy of flow in boundary layer, and controls the boundary layer effectively to increase the circulation of wing. It has been successfully employed in the modern high lift aircraft such as Antonov An-72, MacDonnell Douglas YC-15 and Boeing C-17 Globemaster Ⅲ [4, 5]. Moreover, it is also widely used in helicopter rotor, helicopter tail boom, the guide vane of compressor, turbine cascades, etc [6-8].

Although great efforts have been put into the researches on the mechanism and implementability of CC technology, little information is given about its application for the flight control of flapless aircrafts so far. Wilde used CC devices instead of conventional control surfaces in an experimental study of Boeing X-45A, which is an example of a tailless flight vehicle. Rolling and pitching moments can be produced independently by lateral symmetric operation, and yawing moments can also be realized by simultaneous blowing from upper and lower CC slots at one side of fuselage [9].
In this study, our focus is on obtaining the effect law of blowing moment coefficient and jet position on the performance of circulation control on a flapless UAV, based on which the CC scheme is designed and optimized to achieve the purpose of high efficient, independent and decoupling control of three moment components. The CFX 15.0 software is used for three-dimensional numerical simulation of the aerodynamic characteristics of the UAV with several turbulence models.

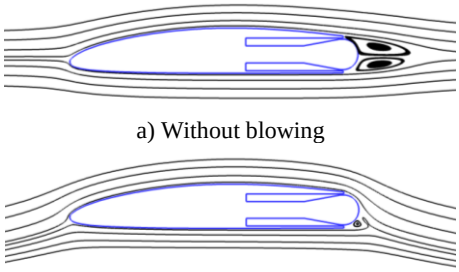

a) Without blowing

b) Blowing from the upper slot

Figure 1: The operational principle of circulation control airfoils

2 Problem Statement

2.1 Geometry and important parameters

The geometric structure of the circulation control vehicle for computation was constructed based on a flapless UAV, the aerodynamic characteristics of which have been experimentally studied in low speed aerodynamics institute, as shown in Figure 2. The vehicle has a tailless and flying-wing configuration, and there are 8 CC units at the trailing edge of wing instead of flaps or ailerons. Each CC unit can work independently with straight blowing slots and semicircle surface as Coanda surface, and the CC units are connected to the on-board compressor through ducts and a Mass-flow Control Unit (MCU), which can adjust total pressure p_j and total temperature T_j in each duct accurately. Moreover, the same sizes of curvature radius R and height h of jet slot are set in all CC units for convenience.

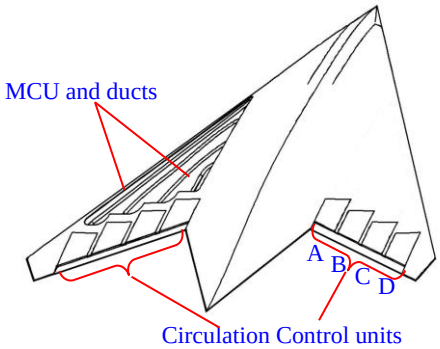

Figure 2: The flapless UAV configuration

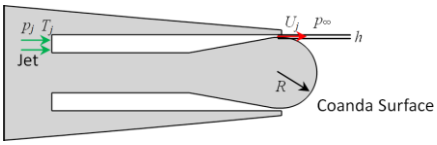

Figure 3: Blowing control unit and Coanda surface at the trailing edge of wing

The average velocity of jet at slot exit U_j can be determined by one-dimensional isentropic equation as [10]

$$U_i = \sqrt{2RT_j\left(\frac{\gamma}{\gamma-1}\right)\left[1-\left(\frac{p_\infty}{p_j}\right)^{(\gamma-1)/\gamma}\right]}$$

Momentum coefficient C_μ is the most important influence parameter on the performance of CC technology, and it is associated with jet parameters and airfoil geometry [11], defined as

$$C_\mu = \frac{\dot{m}U_j}{q_\infty S}$$

where $\dot{m}$ is the mass flow rate, q_∞ is the dynamic pressure, and S is the reference area or chord length. In order to distinguish the blowing form, we define C_μ as positive when blowing from upper slots and negative when blowing from lower slots, although it ought to be dimensionless and positive.

2.2 Computational grid

In the computational domain, the streamwise distances of inlet and outlet from the vehicle are 20 times and 45 times the fuselage length, and the normal distance of far-field from the vehicle is 20 times the fuselage length, as shown in Figure 4. Hexahedral structured grids are used for discretization, and the size of the first layer grid near wall is of the order of 5×10^{-3} mm with total number of grid cell being 2.92×10^{7}.

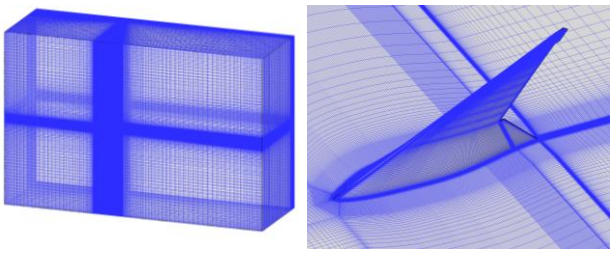
Figure 4: Grid for the flapless UAV

2.3 Control equations, turbulence model and boundary conditions

RANS simulation is applied to obtain the performance of CC on the flapless UAV, and *SST* turbulence model is selected. The far field boundaries above and below the vehicle are set to be velocity inlet, where Mach number is 0.2. The vehicle surface, plenum wall and Coanda surface are all adiabatic walls, and duct entrance is set as pressure inlet. In the computation process, total pressure p_j and total temperature T_j are fixed, which can determine the mass flow rate $\dot{m}$.

2.4 Methods validation

To verify the validity of the numerical simulation method, we selected a two-dimensional CC airfoil NCCR1510-7067N, and simulated its aerodynamic characteristics at angle of attack $\alpha = 0\ deg$. The results are compared with test results from Naval Surface Warfare Center-Carderock Division [12]. As shown in Figure 5, the surface pressure distribution results from numerical simulation are

consistent with experimental data, despite the fact that slight differences exist near the surface suction peak at the trailing edge of airfoil, proving the validation of numerical simulation method.

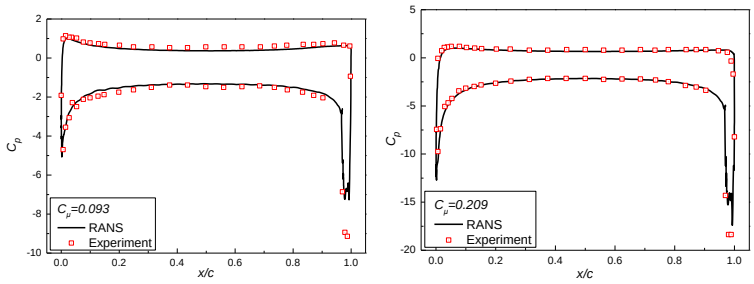

Figure 5: The comparison of airfoil surface pressure distribution

3 Result and Analysis

3.1 Jet position and momentum coefficient

Figure 6 shows the trends of the three control moments in several typical cases. Figure 6(a-b) show that: (1) Blowing from the upper slot with the same momentum coefficient at different positions (A, B, C, D), the pitching moment and rolling moment induced decrease monotonously along the spanwise direction (from position A to D). CC unit A provides the biggest moment increments, although the force arm of unit A for providing control moments is the shortest. (2) Blowing from the lower slot at the same momentum coefficient, CC unit A could also affect the pitching and rolling moment a lot, while the performances at CC units B, C and D are slightly different. Figure 6(c) shows that the yawing moment increment induced increases monotonously along the spanwise direction, opposite to the trend for the pitching moment and rolling moments. Also, all the three increments of moment coefficient increase with increasing momentum coefficient. Comparing the effects of the blowing jet at four exhibition positions, we can conclude CC unit A's contribution to the lift, pitching moment and rolling moment is superior to that of other units. Jet from some lateral CC unit has lager effect on the yawing moment. These understandings from computational results are helpful for the optimization of the CC scheme and the improvement of CC efficiency.

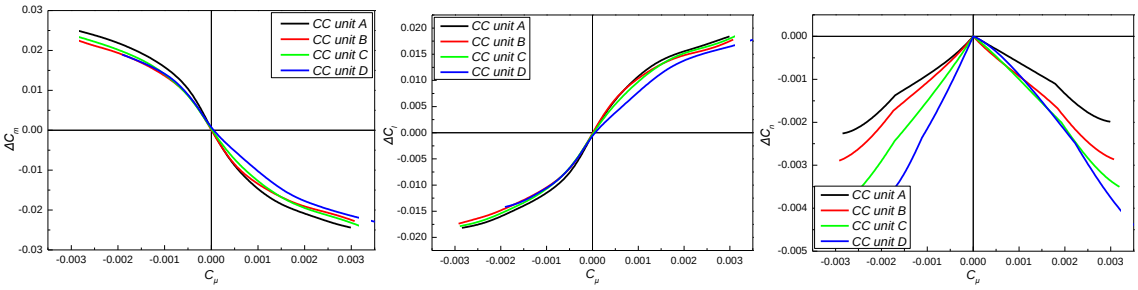

(a) (b) (c)

Figure 6: The influence of blowing position on the performance of circulation control

3.2 Design and optimization of Circulation Control scheme

We now turn to the design and optimization of CC scheme in the current situation of CC units. Considering a subsonic case (Ma=0.2) and zero angle of attack. CC units A, B and C, which are close to the wing root relatively, are combined to realize the pitching and roll control of vehicle. Table 1 lists three types of CC scheme and the duct total pressure p_j for each unit. This section contrasts the CC features of combined-pressure schemes and a uniform-pressure scheme to optimize.

Table 1: The duct total pressure p_j for each unit in the three CC schemes

Type	Unit A	Unit B	Unit C	Unit D
Ⅰ	p_j	p_j	p_j	closed
Ⅱ	$1.1p_j$	$0.8p_j$	$0.8p_j$	closed
Ⅲ	$1.1p_j$	$0.9p_j$	$0.9p_j$	closed

As shown in Figure 7, the increments of pitching moment coefficient and roll moment coefficient increase with increasing C_μ for the three typical CC schemes. Blowing from the upper slots at both sides of the UAV simultaneously, the circulation and lift are seen to increase due to Coanda effect at trailing edge of wing, which results in upward force. With C_μ = 0.008, the increment of pitching moment coefficient ΔC_m = 0.0672. While blowing from the lower slots on both sides, the blowing jet results in downward force. When C_μ = 0.008, the increment of pitching moment coefficient ΔC_m achieves the value of 0.0675. Blowing from the upper slot at the left side of wing and blowing from the lower slot at the right side will make the vehicle roll to the right side of fuselage around the longitudinal axis. With C_μ = 0.008, the increment of roll moment coefficient ΔC_l = 0.0509. On the other hand, the vehicle will roll to the left side around the longitudinal axis if the opposite blowing way is employed (i.e. blowing from the lower slot at the left side of wing and blowing from the upper slot at the right side). Further, the curves indicate that the performances of circulation control are nearly the same for the three schemes, implying that increasing the total pressure can improve the jet velocity at slot exit, but has little effect on the promotion of circulation control performance.

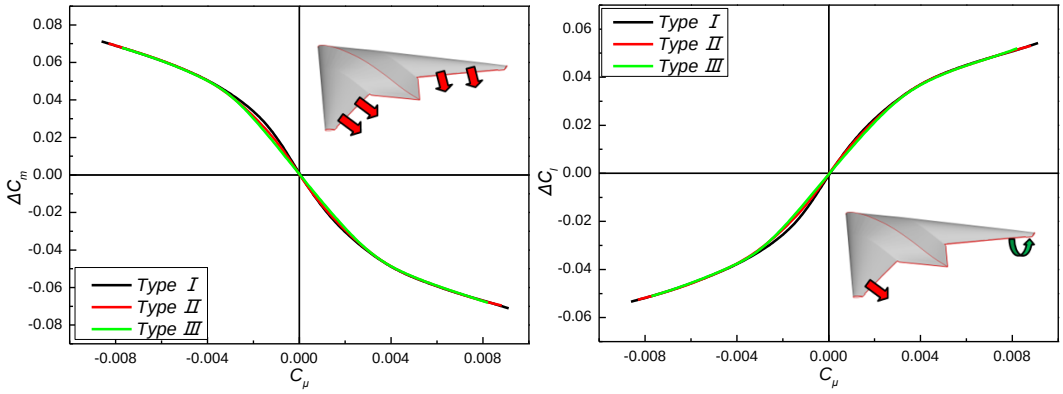

Figure 7: Manipulation moments for pitching and roll control

For yaw control, the values of Ma and α are the same as those considered in pitching and roll control. Further, the lateral CC units C and D are combined for the implementation of yaw control. Table 2 lists two blowing schemes for yaw control. In order to eliminate the additional pitching moment and rolling moment, the pressures are slightly different among different ducts.

Table 2: Two blowing schemes for yaw control

Type	Unit A	Unit B	Unit C	Unit D
Ⅳ	closed	closed	upper and lower	upper and lower
Ⅴ	closed	closed	upper or lower	lower or upper

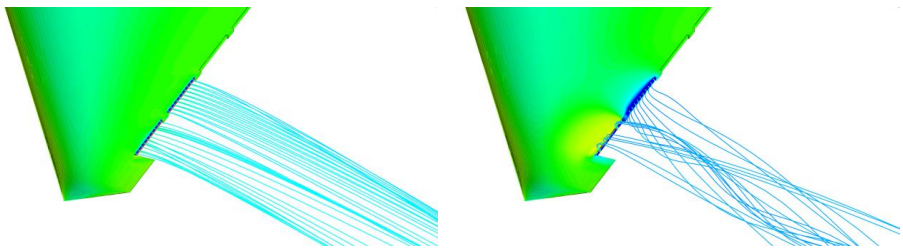

Figure 8: The comparison of streamlines near the trailing edge of wing. Left: type Ⅳ, Right: type Ⅴ.

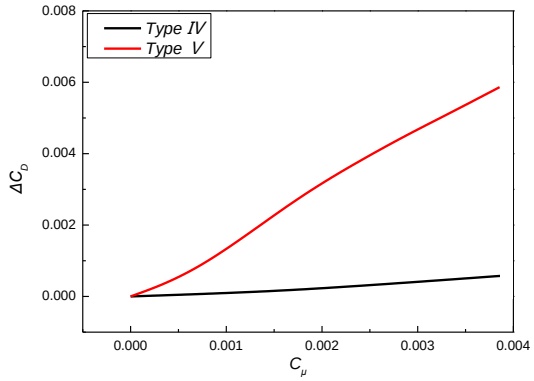

Figure 9: The variation of drag coefficient increment with C_μ in yaw control

Figure 8 shows the comparison of the streamlines near the trailing edge of wing between blowing scheme Ⅳ and Ⅴ. Blowing from both upper and lower slots of CC units C, D simultaneously as in scheme Ⅳ, called as the way of fluidic thrust, the blowing jet can produce independent yawing moment. While blowing from the upper slot of unit C and the lower slot of unit D simultaneously as in type Ⅴ, the vortex appear after the trailing edge. Figure 9 shows the variation of drag coefficient increment with C_μ in yawing control, which indicates that the induced drag by type Ⅴ is much larger than that by type Ⅳ at the same C_μ.

Figure 10 shows the trends of the manipulation moments in yawing control. Figure 10(a-b) show that the increments of pitching and roll moment coefficient are less than 0.001 in the range of C_μ investigated, which can be negligible. Figure 10(c) shows that both scheme Ⅳ and Ⅴ can produce yawing moments, and the increments increase with C_μ respectively. With C_μ = 0.0039, the increments of yawing moment coefficient ΔC_n are 0.00023 and 0.00288 in scheme Ⅳ and Ⅴ, respectively. Thus, it can be concluded that the yawing control schemes help to realize the decoupled control of yawing moment. Although fluidic thrust can also obtain a little yawing moment, it could not reach the requirement of yawing handling, scheme Ⅴ can efficiently obtain sufficient yawing moment coefficient by taking advantage of the increment of induced drag.

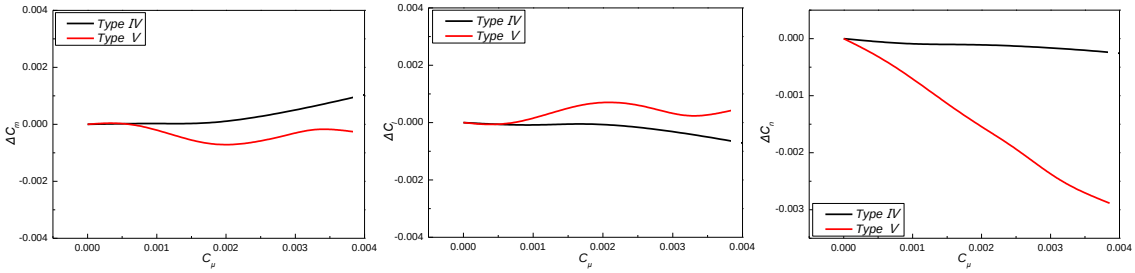

(a) (b) (c)

Figure 10: Manipulation moments in yawing control

4 Conclusion

In this paper, RANS method was utilized to study the circulation control performance on a flapless UAV. The numerical simulation results show that:

(1) Blowing position has played an important role in circulation control performance. The blowing jet close to wing root produces more increments of lift, pitching moment and rolling moment compared with that at other blowing unit. The blowing jets at lateral CC units have lager affect on the yawing moment.

(2) Increasing the duct total pressure can improve local jet velocity at slot exit, but has little effect on the promotion of circulation control performance. Compared with the CC schemes featured by

distributed total pressures at different units, the scheme with uniform total pressure simplifies the fluidic control scheme for the maneuvering control of the vehicle.

(3) The yawing control schemes help to realize the decoupled control of yawing moment.

(4) Although fluidic thrust can also obtain a little yawing moment, it could not reach the requirement of yawing handling. Obviously, using the method of wall-bounded jet to produce the induced drag is more efficient.

Acknowledgments

Support from the National Natural Science Foundation of China under Grants No. 11402284 is gratefully acknowledged.

References

[1] Jones, G. S. *et al*. An active flow circulation controlled flap concept for general aviation aircraft applications. AIAA paper 2002-3157, 2002.

[2] Anders SG, Sellers WL, Washburn AE. Active flow control activities at NASA Langley. AIAA Paper 2004-2623, 2004.

[3] Wood, N. and Nielsen, J. Circulation control airfoils past, present, future. AIAA Paper 1985-0204, 1985.

[4] Leonard R, Tavernetti. The C-17: Modern Aircraft Technology. AIAA Paper 1992-1262, 1992.

[5] Englar, R. J., Smith *et al*. Application of circulation control to advanced subsonic aircraft, part I: airfoil development. J Aircraft, 31(5), 1160–1168, 1994.

[6] Lin Li. Development of helicopters. *Aviation Industry Press*, 168-172, 2007.

[7] Hill, H. *et al*. 2D Parametric study using CFD of a circulation control inlet guide vane. ASME paper GT2007-28058, 2007.

[8] Y. Song, Y. Li, H. Chen, F. Chen. Two-dimensional simulation of circulation control turbine cascade. *Journal of Aerospace Engineering*, 225(7): 761-767, 2011.

[9] P. I. A. Wilde, W. J. Crowther, C. D. Harley. Application of circulation control for three-axis control of a tailless flight vehicle. *Journal of Aerospace Engineering*, 224, Part G: 373-385, 2010.

[10] Englar, R. J. Two-dimensional subsonic wind tunnel tests of two 15-percent thick circulation control aerofoils. *Tech. Rep.* AL-211. NSRDC. 1971.

[11] G. S. Jones, C. Yao, B. G. Allen. Experimental investigation of a 2-D supercritical circulation control airfoil using particle image velocimetry. AIAA 2006-3009, 2006.

[12] J. Abramson. Two-dimensional subsonic wind tunnel evaluation of two related cambered 15-percent-thick circulation control airfoils, *Technical report*, DTNSRDC, 1977.